Nuclear Instruments and Methods in Physics Research B 372 (2016) 156–160

Contents lists available at ScienceDirect

Nuclear Instruments and Methods in Physics Research B

journal homepage: www.elsevier.com/locate/nimb

Vacancy-related defects in *n*-type Si implanted with a rarefied microbeam of accelerated heavy ions in the MeV range

I. Capan [a], Ž. Pastuović [b,*], R. Siegele [b], R. Jaćimović [c]

[a] Rudjer Boskovic Institute, Bijenička 54, 10000 Zagreb, Croatia
[b] Center for Accelerator Science, ANSTO, Locked bag 2001, Kirrawee Dc, NSW 2232, Australia
[c] Jozef Stefan Institute, Jamova Cesta 39, 1000 Ljubljana, Slovenia

ARTICLE INFO

Article history:
Received 23 September 2015
Received in revised form 2 December 2015
Accepted 21 December 2015
Available online 13 February 2016

Keywords:
Ion implantation
Silicon
Defects
Vacancy
DLTS

ABSTRACT

Deep level transient spectroscopy (DLTS) has been used to study vacancy-related defects formed in bulk *n*-type Czochralski-grown silicon after implantation of accelerated heavy ions: 6.5 MeV O, 10.5 MeV Si, 10.5 MeV Ge, and 11 MeV Er in the single ion regime with fluences from 10^9 cm^{-2} to 10^{10} cm^{-2} and a direct comparison made with defects formed in the same material irradiated with 0.7 MeV fast neutron fluences up to 10^{12} cm^{-2}. A scanning ion microprobe was used as the ion implantation tool of *n*-Cz:Si samples prepared as Schottky diodes, while the ion beam induced current (IBIC) technique was utilized for direct ion counting. The single acceptor state of the divacancy $V_2(-/0)$ is the most prominent defect state observed in DLTS spectra of *n*-CZ:Si samples implanted by selected ions and the sample irradiated by neutrons. The complete suppression of the DLTS signal related to the double acceptor state of divacancy, $V_2(=/-)$ has been observed in all samples irradiated by ions and neutrons. Moreover, the DLTS peak associated with formation of the vacancy-oxygen complex VO in the neutron irradiated sample was also completely suppressed in DLTS spectra of samples implanted with the raster scanned ion microbeam. The reason for such behaviour is twofold, (i) the local depletion of the carrier concentration in the highly disordered regions, and (ii) the effect of the microprobe-assisted single ion implantation. The activation energy for electron emission for states assigned to the $V_2(-/0)$ defect formed in samples implanted by single ions follows the Meyer–Neldel rule. An increase of the activation energy is strongly correlated with increasing ion mass.

1. Introduction

The generation of complex defects is certainly among the most fundamental mechanisms for degradation of the silicon electronic properties. The radiation-induced defects, with their energy levels in the bandgap, can give rise to following processes involving free charge carriers: generation, recombination, trapping, compensation, tunnelling, scattering, type conversion, and field enhanced carrier generation [1]. In principle, any combination, or all, of these processes can occur through the same level. The role a particular level plays depends on variables such as carrier concentration, temperature, or position where it resides in a device (e.g., in a depletion region). These deep defects are mostly created by the non-ionizing energy loss (NIEL) processes, which generate primary defects by the initial particle interaction and by the cascade generation due to the recoil silicon atom [2]. It is well known that the performance of silicon devices which are operated, e.g. used for detection and monitoring of the ionizing radiation, in harsh radiation environments associated with the outer space, nuclear reactors or accelerator-based research facilities, degrades with an increasing accumulated fluence of any particle radiation. The rate of degradation for a particular device strongly depends on irradiation conditions such as type and energy of particles, particle flux, particle fluence, and temperature [1,3–5].

Radiation damage testing procedures of devices used or intended for usage in those environments usually require large doses of low ionizing particles and corresponding long exposure times. An alternative testing methodology utilizes the accelerated ion beam, with energies in the MeV range, for irradiation of a device in order to simulate the radiation damage created by high energy neutrons, protons, pions, electrons, etc. Ions having an energy of 0.1–1 MeV per mass unit have an advantage of the higher NIEL energy deposition per particle compared to low ionizing particles [4,6,7]. Therefore defect concentrations required for

* Corresponding author.
E-mail address: zkp@ansto.gov.au (Ž. Pastuović).

http://dx.doi.org/10.1016/j.nimb.2015.12.039
0168-583X/© 2016 Published by Elsevier B.V.

testing purposes can be achieved with much lower particle fluence values and thus shorter exposure times.

The capability of ion microprobes [8] to perform high-flux, high-frequency and high-precision scanning of an ion microbeam, compared to conventional ion broad-beam sources offer advantages of: (a) selecting a particular region of interest on the device, (b) a computer controlled positioning of an ion microbeam, (c) minimising irradiation area size, (d) rapid irradiations minimising exposure times and (e) single ion implantation [9]. The high vacancy generation rates in discrete highly disordered regions where a massive energetic projectile like a heavy ion collides with a lattice atom and creates a secondary recoil cascade increase the probability for formation of vacancy related defects in *n*-type silicon. Vacancy-related defects are the most dominant electrically active defects in *n*-type silicon produced by ion implantation. It is known that vacancy-related defects introduce three electronic states in the upper part of the band gap. The vacany-oxygen (VO) pair, double negatively charge state of divacancy $V_2(=/-)$, and single negatively charge state of divacancy $V_2(-/0)$ are associated with levels at 0.18, 0.23 and 0.43 eV, respectively [10]. It has been observed that the divacancy has different behaviour when *n*-type Si is irradiated with electrons, neutrons or implanted with heavy ions [11]. For divacancy formation, the migration length of monovacancies may not be very crucial. The migration length of vacancies has been estimated to be in the order of ~100 nm in Cz and float-zone Si [12]. Assuming a simplified model for divacancy formation as a reaction of pairing of monovacancies ($V + V \rightarrow V_2$), one can conclude that divacancies are predominantly formed in the cascade cores because the formation rate depends quadratically on the monovacancy concentration. Moreover, it is known that V_2 can be generated directly in a primary collision event without any subsequent migration [13]. We already showed that using a single ion implantation by rarefied ion microbeam (~kHz ion rate) at the room temperature, in the low level radiation damage approximation, the stable final defects are mainly formed from only primary point defects generated within each ion cascade [14]. Moreover, the depth profiling of ion implanted *n*-type silicon by the DLTS showed that the single acceptor state of divacancy is the most dominant defect created within the end of an ion range. For the low *Z* ion implantation like oxygen the formed divacancies are isolated point defects, while for the heavier ions like silicon we observed the broadening of the $V_2(-/0)$ state. The measurements of the capture cross section for the $V_2(-/0)$ state didn't show results typically obtained for the point defects, i.e. discrete divacancies, but revealed the complex structure of divacancy states attributed to the small divacancy clusters [14]. Formation of small vacancy and interstitial clusters with energy levels very close to the energy of the single acceptor state of divacancy was previously also observed in the Laplace DLTS study of heavy ion implanted *n*-type silicon with doses up to $10^9\,\mathrm{cm}^{-2}$ by Abdelgader and Evans-Freeman [15].

The main aim of this work is to further investigate the vacancy-related defects formed in low-doped *n*-type silicon as a result of single heavy ion implantation with energies in the MeV range.

2. Experimental details

For this study we used the *n*-type silicon Schottky diodes produced on phosphorus-doped Czohralski-grown (CZ) (100) silicon wafers with specified initial resistivity of 30 Ω cm. The Schottky contacts were formed by the thermal evaporation of gold, while the Ohmic contacts were formed by the thermal evaporation of aluminium on the back side of silicon wafer. Details are given elsewhere [16]. The quality of the prepared diodes was characterized by *I*–*V* and 1 MHz *C*–*V* measurements at different temperatures (77–300 K). The uniformity of charge collection efficiency in the Schottky diodes was checked with the IBIC microscopy [17] prior to the irradiation. The diode design (size, doping and thicknesses) and irradiation conditions have been optimised for the direct single ion counting by the IBIC technique and the DLTS analysis of the implanted samples. The samples were homogenously implanted by 6.5 MeV $^{16}O^{2+}$, 10.5 MeV $^{28}Si^{3+}$, 10.5 MeV $^{72}Ge^{3+}$, and 11 MeV $^{167}Er^{4+}$at the ANSTO heavy ion microprobe facility capable of focusing ions with the maximum rigidity of ME/q2 = 120 [18]. The ion species and energies were chosen to obtain the similar end of an ion range. The corresponding ion fluences in the 10^9–$10^{10}\,\mathrm{cm}^{-2}$ range result in approximately similar total energy deposited for displacements of target silicon atoms by various ions according to the NIEL hypothesis [4]. The microbeam with ion rate $5 \times 10^{11}\,\mathrm{cm}^{-2}\mathrm{s}^{-1}$ was raster scanned multiple times over an area of approximately 500 μm × 500 μm to avoid the instantaneous implantation of the full dose and achieve a more homogenous ion implantation. The scan area was divided in 512 × 512 pixels, i.e. each pixel size is approximately 1 μm × 1 μm. A dwell time per pixel was equal to 1 ms, i.e. on the average 5 ions were implanted in each pixel before the microbeam was moved to the next pixel position. A negligible error of the calculated fluence values might be caused by a dead time of DAQ system.

For comparison a set of samples was irradiated with 0.7 MeV neutrons in the carousel facility (CF) of the TRIGA Mark II reactor of the Jozef Stefan Institute in Ljubljana, Slovenia. Neutron irradiations were done inside a cadmium box with thickness of 1 mm to filter out the thermal neutrons. The effective cut-off energy of Cd is 0.55 eV, with distribution maximum for fast neutrons at 0.7 MeV [19]. The accumulated fluence of fast neutrons was $10^{12}\,\mathrm{cm}^{-2}$. The temperature of the samples during irradiation did not exceed 30 °C.

Deep defects created in the bulk material after the ion implantation and the neutron irradiation were characterized with the Sula Technologies spectrometer. The DLTS measurements were performed at temperatures between 77 and 300 K. Eight different rate windows were used in order to determine the defect DLTS signature (activation energy for electron emission and capture cross section).

3. Results and discussion

Fig. 1 shows the primary monovacancy generation rates calculated by SRIM [20] for five different 10.5 MeV Ge single ions implanted in a silicon target through 100 nm thick Au surface layer. The incident angles of 0, ±1/2°, and ±1° have been chosen to match the spatial properties of focused ion microbeam (represented with a cone 160 mm in length, 2 mm across its base and a finite tip size of ~1 μm) and the statistical nature of the process. From projections of cumulative primary monovacancy distribution in a plane parallel with a beam axis (Fig. 1a–d and f) we can estimate that the atomic displacements are confined to a relatively narrow cylindrical region of ~50 nm in cross section along the cascades which is consistent with results molecular dynamics simulations of low-energy heavy-ion implantation in Si at RT, which predict formation of amorphous zones, with the same lateral size [21]. Comparing those five cascades, also shown together in the surface plot (Fig. 1e), it is obvious that: (i) the cascades diverge one from another having a different secondary cascade depth distribution and (ii) the distribution of monovacancies in a single cascade has a considerable non-uniformity. A weak cascade overlapping close to the surface can be neglected because for the calculation ion-projectiles have the same entrance point which might not be true in reality. The figure shows, that within the track of a single heavy ion there are many separated regions with

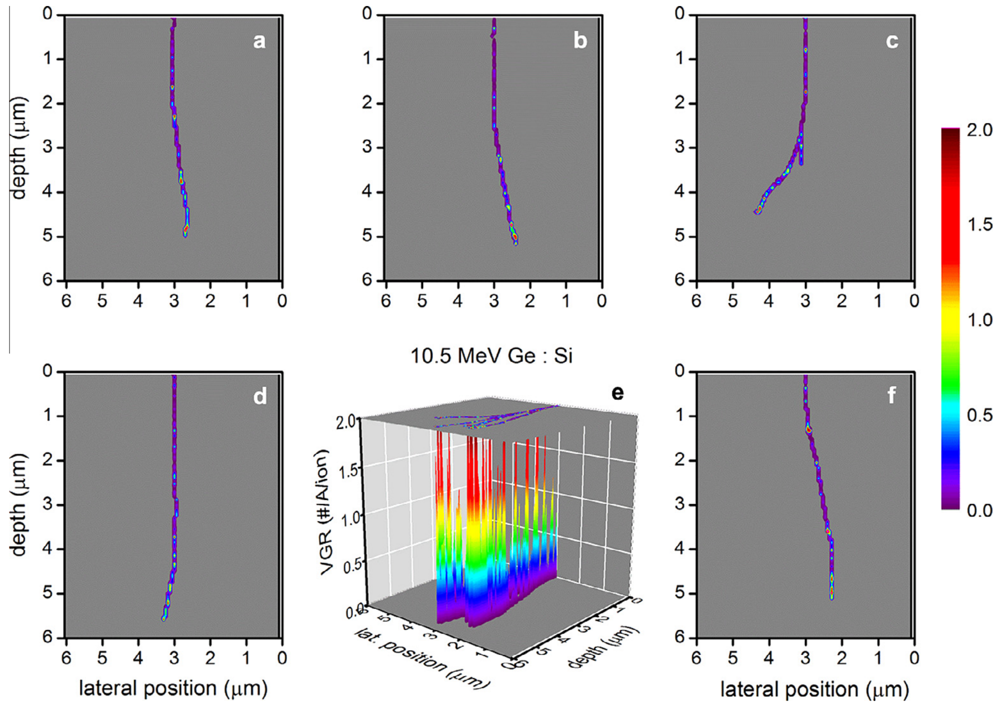

Fig. 1. SRIM simulations of the vacancy generation rates (in units of A^{-1} per ion) for 10.5 MeV Ge single ions implanted in silicon through a 100 nm thick surface Au layer. Fig. 1a–d and f show a projection of the vacancy distribution in a plane parallel with a beam axis for 5 ion-projectiles incident at angles $\alpha = 0, \pm 1/2°$, and $\pm 1°$ respectively. Fig. 1e shows the same projection of cumulative vacancy distribution generated by those 5 ions with specified entering angles into the silicon target.

extremely high densities of one to two monovacancies per angstrom of depth, corresponding to secondary cascades. Due to these highly disordered regions rich with vacancies (concentrations of the order of up to 10^{18} cm^{-3} for Ge ion) it is expected that predominantly vacancy related defects will be formed. Fig. 2 compares the average monovacancy generation rates (10,000 ions used for each SRIM simulation) for different ions in this work.

Svensson et al. observed a decrease of defect generation rate with an increased ion flux [22], which suggests that the recovery process is hastened by the irradiation. One obvious mechanism for this is the local heating produced by the passage of bombarding radiation – the thermal spike model proposed by Seitz [23], in which a moving particle heats up the material surrounding its track through the solid. It seems likely that in most cases the duration of a heating process of the order of 10^{-12} sec is too brief

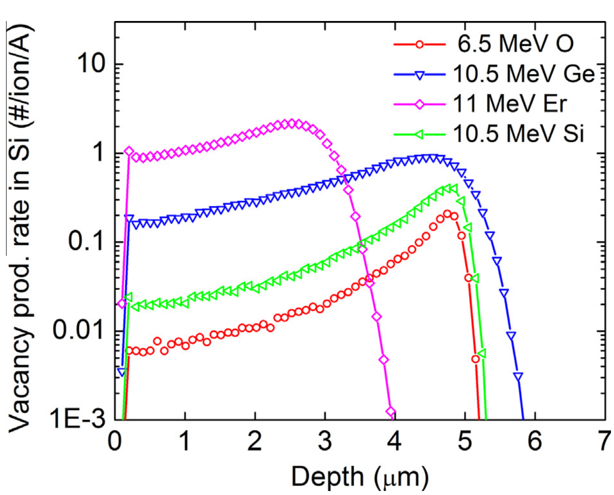

Fig. 2. The average vacancy generation rate per unit length in silicon for selected ions penetrating through 100 nm thick surface Schottky contact made of evaporated gold.

to produce appreciable recovery. Koehler and Seitz [24] suggest that the excitation of electrons facilitates the movements of interstitials or vacancies. It is also possible that collisions move the vacancies and interstitials.

The threshold energy for such movements is much less than the 21 eV required for displacement of a silicon atom [25] and consequently the probability of moving an interstitial or a vacancy is much larger than the probability of forming it in the first place. Thus the broad beam ion irradiation where the total sample area is irradiated at once (and the whole sample is simultaneously heated by the ion beam) may induce movements which are large compared with thermally activated movements, and produce a recovery which would not occur in the absence of radiation.

But, it is also important to once again highlight a unique feature of the scanning rarefied ion microbeam used in our irradiation experiment: the average time between two ion hits in the same pixel is ~200 µs, which is much longer than duration of a thermal spike. Therefore, the thermally stimulated recovery or reorganization of final defects as a result of additional radiation annealing from demonstrated weakly overlapping cascades is reasonable to be assumed negligible. In a conclusion, the final defect species which are formed from primary defects generated in locally disordered regions along ion cascades can be considered a result of the single ion hit. The calculated free carrier concentration in a pristine device is of the order of 10^{14} cm^{-3} (Fig. 3). The cumulative decrease of the free carrier concentration across the whole section from surface to the extent of implantation range is supporting the fact that traps which capture free electrons are formed in irradiated devices. Fig. 4 shows DLTS spectra of phosphorus-doped CZ-grown silicon irradiated with fast neutrons (0.7 MeV) and 6.5 MeV O, 10.5 MeV Si, 10.5 MeV Ge, 11 MeV Er ions. The spectra have been vertically displaced for clarity. All measurements are recorded upon irradiation and no annealing has been carried out. The neutron flux was chosen based on the simulation results, in order to introduce the same amount of the vacancy-related defects (compared to Si ion implantation). Two deep traps with their DLTS peak maxima at

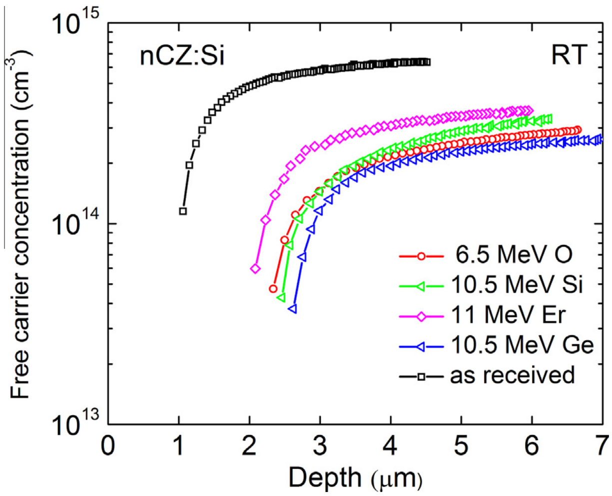

Fig. 3. Free carrier concentration estimated from the 1 MHz C–V measurements at room temperature.

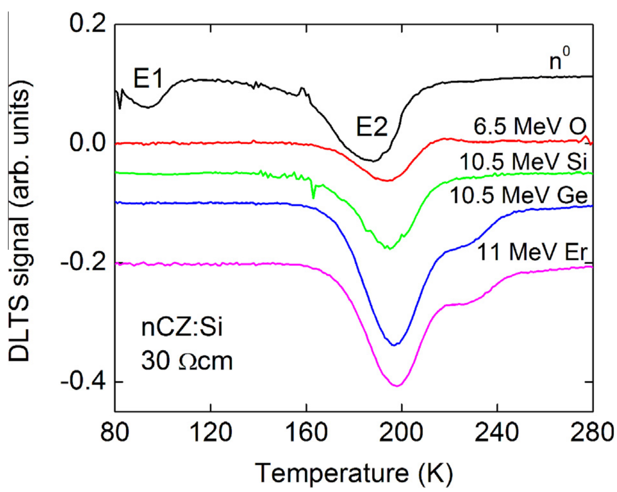

Fig. 4. DLTS spectra for all samples, fast neutron irradiated and ion implanted, measured with the emission rate 4.65 s^{-1}, reverse bias −5 V → −0.2 V and pulse duration 10 ms. The spectra are vertically shifted for the clarity.

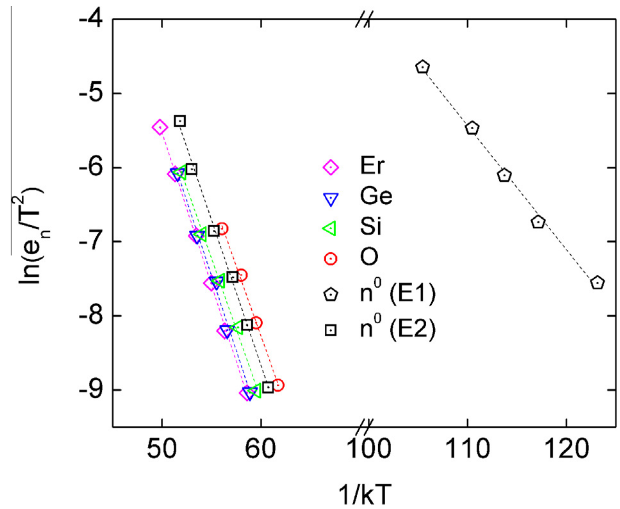

Fig. 5. Arrhenius plots of T2-corrected emission rates for all observed defects. Electronic parameters derived from the plots are given in Table 1.

about 92 and 188 K for an emission rate window of 4.65 s^{-1} are observed in the spectrum of the fast neutron irradiated sample. One prominent defect state corresponding to DLTS maximum at around 196 K has been observed in all ion-implanted samples. Arrhenius plots of T^2-corrected emission rates for all observed traps which act as electron traps are shown in Fig. 5. Obtained values for the activation energy for electron emission (ΔE_{ne}), the pre-exponential factor (A_{ne}) and the capture cross section, together with the defect identification, are given in the Table 1. The calculated energy levels of traps observed in the neutron-irradiated sample are in agreement with well-established values in the literature [10,11]. Therefore those traps have been assigned to the VO (−/0) and V_2(−/0) defects. For the low phosphorous-doped silicon wafers, as the one used in our study with [P] of the order of 10^{14} cm^{-3}, the formation of vacancy-phosphorus complex state (VP defect) can be neglected [26]. The DLTS peak related to the V_2(−/0) defect exhibits an asymmetric broadening; a feature, which is usually associated with more complex defects [27]. Another interesting feature has been detected upon fast neutron irradiation, and that's the suppression of the DLTS peak related to the double acceptor state of divacancy V_2(=/−). It is a well-known fact that for neutron irradiation [10] and ion implantation [28], the ratio between DLTS signals associated with two charge states of divacancy is changing, compared to the electron irradiation when the intensity of DLTS signals originated from both charge states is equal. Moreover, it is already reported by Vines et al. [29] that DLTS intensities of VO(−/0) and V_2(=/−) related traps are decreasing after He, C, Si and I implantations. In particular, the DLTS signal originating from V_2(=/−) defect is almost completely vanished after the I implantation, as the suppression is correlated with increasing ion mass.

Table 1
Activation energies for electron emission, pre-exponential factor and the capture cross section for all observed traps derived from Arrhenius plots.

Damaging particle	Activation energy/eV	Defect identification	Pre-exponential factor (s^{-1} K^{-2})	Capture cross-section (cm^2)
6.5 MeV O	0.38 ± 0.01	V_2(−/0)	9.37×10^5	2×10^{-15}
10.5 MeV Si	0.39 ± 0.02	V_2(−/0)	1.67×10^6	5×10^{-15}
10.5 MeV Ge	0.40 ± 0.02	V_2(−/0)	2.45×10^6	6×10^{-15}
11 MeV Er	0.41 ± 0.01	V_2(−/0)	3.37×10^6	6×10^{-15}
n^0 (E1)	0.17 ± 0.01	VO(−/0)	4.31×10^5	2×10^{-14}
n^0 (E2)	0.39 ± 0.01	V_2(−/0)	1.55×10^6	5×10^{-15}

It should be noted that obtained values for the activation energies of the V_2(−/0) defect observed in all irradiated samples (Table 1) are slightly lower than the benchmark value [30] in some cases, but within the range of reported experimental deviations. Moreover, similar values for the carrier capture cross section (at least the same order of magnitude) justify an assumption of the same defect state. Comparing results in Table 1 with the literature data, we have assigned the most dominant electron trap in all ion implanted samples to the single acceptor state of divacancy V_2(−/0). In our previous study [14], we have already observed a similar effect, the suppression of DLTS signals related to the VO (−/0) and V_2(=/−) defects upon single ion 8.3 MeV Si implantation. We have also shown that in the self-implanted silicon the prominent broad trap with the calculated activation energy for electron emission of 0.4 eV, and related to the V_2(−/0) defect, comes from the closely spaced singly charged divacancies which are formed directly from the nearest monovacancies originating from the single ion impact cascade [14]. These results agree with the model of local compensation of the carrier concentration in highly disordered regions located within the ion cascade region. Results presented in Fig. 4 confirm our previous findings.

Moreover, two interesting features have been observed: (i) the shift of the V_2(−/0) related DLTS peak maxima to the higher

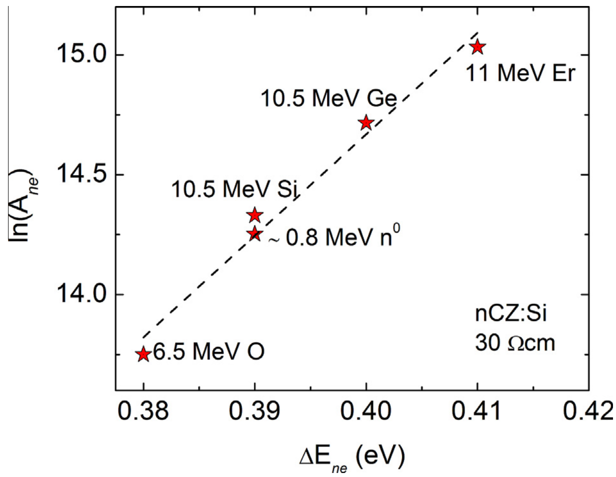

Fig. 6. The pre-exponential factor as a function of the activation energy for electron emission for the $V_2(-/0)$ defect in ion implanted (O, Si, Ge, Er) and fast neutron irradiated samples.

temperatures (which subsequently leads to an increase of the activation energy, Table 1) with the increasing ion mass, and (ii) the appearance of the high temperature shoulder upon heavy ion implantations. The existence of the new deep defect state which captures an electron, evidenced as the high temperature shoulder of the prominent DLTS peak of the $V_2(-/0)$ defect state, is observed upon Ge ion implantation, but it is more clearly visible upon Er ion implantation. However, we have not been able to reliably estimate values for the activation energy and capture cross section for this newly observed state. To our best knowledge, this defect has not yet been reported or identified in the literature. Further studies are needed to clarify the identity of these electron traps.

To further check the behaviour of the observed vacancy-related defects, we have compared the measured values of ΔE_{ne} and A_{ne} for the $V_2(-/0)$ related defect in the fast neutron irradiated sample and in all ion implanted samples. The Meyer–Neldel rule connects the similar thermally activated processes, and is used in distinguishing different types of defects. According to the Meyer–Neldel rule [31], the $\ln(A_{ne})$ should be a linear function of ΔE_{ne} for the same type of defects. Comparing the measured values (Table 1) for the dominant defect in all samples, which we have assigned to the $V_2(-/0)$ (Fig. 4), shows an excellent linear correlation, as shown in Fig. 6. The fact that values obtained upon neutron irradiation fit perfectly within results obtained upon ion implantation strongly supports the conclusion that the observed defects in all samples are indeed related to the $V_2(-/0)$ defect. As already mentioned, the activation energy for electron emission from the $V_2(-/0)$ defect is slightly increasing as the mass of the implanted ions is increasing. Heavy ions produce, more complex cascade regions, more complex defects, which lead to the broadening of the DLTS spectra and therefore have an effect on the estimated activation energy. The ion mass effect on vacancy-related defects in the *n*-type CZ silicon implanted with heavy ions has been reported by Vines et al. [29]. Together with a decrease of the intensity of DLTS peaks related to the VO and $V_2(=/-)$ defects with increasing ion mass, the capture cross section measurements for the $V_2(-/0)$ defect have shown a change in the defect kinetics from the point-like to the extended as a function of the ion mass.

4. Conclusions

We have shown that the single heavy ion implantation leads to the formation of dominant electron trap assigned to the single acceptor state of divacancy $V_2(-/0)$. Broadening of the DLTS peak originating from $V_2(-/0)$ defects formed in the single heavy ion implanted silicon is ascribed to divacancy perturbed by local environments of close lying point defects. The complete suppression of DLTS signal originating from the VO(−/0) and $V_2(=/-)$ defects in the low-doped *n*-type silicon implanted by single heavy ions can be explained by (i) the local depletion of the carrier concentration in the highly disordered regions, and (ii) the effect of the microprobe-assisted single ion implantation. The calculated activation energies for electron emission for the $V_2(-/0)$ related traps observed upon MeV's implantation of O, Si, Ge and Er into Si follows the Meyer–Neldel rule. A slight increase of the activation energy for the electron emission for the $V_2(-/0)$ defect is correlated with increasing ion mass.

Acknowledgments

The authors wish to acknowledge the support of the Croatian Centre of Excellence for Advanced Materials and Sensing Devices, the Accelerator Science Project (0208) and the IAEA CRP #F11016:, Utilization of ion accelerators for studying and modelling of radiation induced defects in semiconductors and insulators.

References

[1] J.R. Srour, C.J. Marshal, P.W. Marshal, IEEE Trans. Nucl. Sci. 50 (3) (2003) 653.
[2] G.H. Kinchin, R.S. Pease, Rep. Prog. Phys. 18 (1955) 1.
[3] G. Lindstrom, Nucl. Instr. Meth. A 512 (2003) 30.
[4] S.R. Messenger, E.A. Burke, G.P. Summers, M.A. Xapsos, R.J. Walters, E.M. Jackson, B.D. Weaver, IEEE Trans. Nucl. Sci. 46 (6) (1999) 1595.
[5] C. Leroy, P.G. Rancoita, Rep. Prog. Phys. 70 (2007) 493.
[6] G.P. Summers, E.A. Burke, P. Shapiro, S.R. Messenger, R.J. Walters, IEEE Trans. Nucl. Sci. 40 (6) (1993) 1372.
[7] A. Chilingarov, D. Lipka, J.S. Meyer, T. Sloan, Nucl. Instr. Meth. A 449 (2000) 277.
[8] M.B.H. Breese, G.W. Grime, F. Watt, Ann. Rev. Nucl. Part. Sci. 42 (1992) 1.
[9] Z. Pastuovic, M. Jaksic, G. Kalinka, M. Novak, A. Simon, IEEE Trans. Nucl. Sci. 56 (2009) 2457.
[10] I. Kovačević, V.P. Markevich, I.D. Hawkins, B. Pivac, A.R. Peaker, J. Phys.: Condens. Matter 17 (2005) S2229.
[11] R.M. Fleming, C.H. Seager, D.V. Lang, E. Bilejec, J.M. Campbell, J. Appl. Phys. 104 (2008) 083702.
[12] K.K. Larsen, V. Privitera, S. Coffa, F. Priolo, S.U. Campisano, A. Carnera, Phys. Rev. Lett. 76 (1996) 1493.
[13] J.W. Corbett, G.D. Watkins, Phys. Rev. Lett. 7 (1961) 314.
[14] Z. Pastuovic, I. Capan, R. Siegele, R. Jacimovic, J. Forneris, D.D. Cohen, E. Vittone, Nucl. Instr. Meth. B 332 (2014) 298.
[15] N. Abdelgader, J.H. Evans-Freeman, J. Appl. Phys. 93 (9) (2003) 5118.
[16] B. Novoselnik, M. Pilipovic, R. Jacimovic, B. Pivac, R. Slunjski, I. Capan, Nucl. Instr. Meth. B 268 (2010) 2400.
[17] M.B.H. Breese, E. Vittone, G. Vizkelethy, P.J. Sellin, Nucl. Instr. Meth. B 264 (2007) 345.
[18] R. Siegele, D. Cohen, N. Dytlewski, Nucl. Instr. Meth. B 158 (1999) 31.
[19] B.E. Watt, Phys. Rev. 87 (1952) 1037.
[20] http://www.srim.org.
[21] M.J. Caturla, T. Diaz de la Rubia, G.H. Gilmer, Nucl. Instr. Meth. B 106 (1995) 1.
[22] B.G. Svensson, C. Jagadish, A. Hallen, J. Lalita, Phys. Rev. B 55 (1997) 10498.
[23] F. Seitz, Rev. Mod. Phys. 26 (1954) 7.
[24] J.S. Koehler, F. Seitz, Z. Phys. 138 (1954) 238.
[25] J.W. Corbett, G.D. Watkins, Production of divacancies and vacancies by electron irradiation of silicon, Phys. Rev. 138 (1965) A555.
[26] G.D. Watkins, J.W. Corbett, Phys. Rev. 134 (1964) A1359.
[27] I. Capan, V. Borjanović, B. Pivac, Solar Energy Mater. Solar Cells 91 (2007) 931.
[28] E.V. Monakhov, J. Wong-Leung, A.Yu. Kuznetsov, C. Jagadish, B.G. Svensson, Phys. Rev. B 65 (2002) 245201.
[29] L. Vines, E.V. Monakhov, J. Jensen, A.Yu. Kuznetsov, B.G. Svensson, Phys. Rev. B 79 (2009) 075206.
[30] B.G. Svensson, B. Mohadjeri, A. Hallen, J.H. Svensson, J.W. Corbett, Phys. Rev. B 43 (1991) 2292.
[31] V.P. Markevich, I.D. Hawkins, A.R. Peaker, K.V. Emtsev, V.V. Emtsev, V.V. Litvinov, L.I. Murin, L. Dobaczewski, Phys. Rev. B 70 (2004) 235213.